Supporting Information for:

Rectification in Molecular Tunneling Junctions based on Alkanethiolates with Bipyridine-Metal Complexes

Junwoo Park,[1] Lee Belding,[1] Li Yuan,[1] Maral P. S. Mousavi,[1] Samuel E. Root,[1] Hyo Jae Yoon,[1,2] and George M. Whitesides[1*]

[1] Department of Chemistry and Chemical Biology, Harvard University, 12 Oxford Street, Cambridge, MA 02138, United States

[2] Department of Chemistry, Korea University, Seoul 02841, Korea

* Corresponding author E-mail: gwhitesides@gmwgroup.harvard.edu

Nomenclature

We use the notations "Au^{TS}-$S(CH_2)_{11}$BIPY-Co//Ga_2O_3/EGaIn" and "Au^{TS}-$S(CH_2)_{11}$BIPY-Cu//Ga_2O_3/EGaIn" to describe the molecular junctions. Here, "Au^{TS}" represents template-stripped (TS) gold surface as a bottom electrode and "EGaIn" represents eutectic indium-gallium (EGaIn, 75.5 % Ga 24.5 %, and a superficial layer of GaO_x) alloy as a top electrode.[1,2] We denote the 4-methyl-2,2'-bipyridine (BIPY) terminated-SAMs as $S(CH_2)_{11}$BIPY,[3] and SAMs of $S(CH_2)_{11}$BIPY complexed with Co(II)Cl_2 and Cu(II)Cl_2 as $S(CH_2)_{11}$BIPY-Co and $S(CH_2)_{11}$BIPY-Cu, respectively. We use the symbols "//" to indicate a non-covalent interface, and "/" to indicate an interface between EGaIn and Ga_2O_3.[4,5] HOMO stands for highest occupied molecular orbital, and LUMO stands for lowest unoccupied molecular orbital.

Experimental Details

Materials All reagents were used as supplied unless otherwise specified. All organic solvents in analytical grade (99%) were purchased from Sigma-Aldrich. The 1-octadecanethiol was purchased from Sigma-Aldrich (>98% purity). High purity eutectic gallium-indium (EGaIn; 99.99%) was obtained from Sigma-Aldrich and used as supplied.

Preparation of 2,2'-Bipyridyl-terminated n-Undecanethiol. Our synthesis of the BIPY-containing SAMs that consist of an insulating alkyl chain and a BIPY moiety followed a literature procedure.[3]

Preparation of Junctions. SAMs of $S(CH_2)_{11}$BIPY were formed by immersion of a smooth template-stripped (TS) gold surface (Au^{TS}) in 1.0-mM ethanolic solutions of thiol-terminated molecules for 18 hours under a nitrogen atmosphere. The BIPY moieties complexed with metal (II) on incubation with a 10-mM solution of metal(II) chloride in ethanol to form

Au^{TS}-$S(CH_2)_{11}$BIPY-M junctions under a nitrogen atmosphere for 18 hours. After each immersion, we gently rinsed the samples with ethanol for one minute to remove residue on the surface, and dried the samples under a slow flow of nitrogen gas.

Characterization: J-V Measurements. We performed the measurements within one hour after the samples were prepared. After positioning the samples (Au^{TS}-$S(CH_2)_{11}$BIPY-Co and Au^{TS}-$S(CH_2)_{11}$BIPY-Cu) on the anti-vibration table, we connected a grounded Au surface to the negative port of a source meter (6430 Sub-Femtoamp Remote SourceMeter, Keithley). A 10-μL Hamilton syringe containing eutectic indium-gallium (EGaIn, 75.5 % Ga 24.5 %, and superficial layer of GaO_x) alloy serving as a top electrode was controlled by a micromanipulator, and was connected to the port of the source meter. We formed an EGaIn tip of conical shape by extruding an EGaIn drop from the syringe on a clean Si wafer,[2,6] and brought the EGaIn tip gently into contact with the samples (contact area ~ 900 μm^2). A bias voltage was subsequently applied to the EGaIn tip (positive bias corresponds to EGaIn oxidizing and negative bias corresponds to EGaIn reducing), and measured current flowing across the junctions (one trace from -1.0 V to 1.0 V).

Statistics. Detailed descriptions of the statistical analysis of the data have been reported,[7] and we followed a standard protocol for the data analysis. Here is brief description of the overall procedure: For the characterization of the molecular junctions, we fabricated four samples separately. Then, we obtained J-V traces from the samples by measuring 4 or 5 junctions on each sample and collecting 21 J-V traces per junction. The J-V traces are obtained by averaging all measured traces. As we defined, the rectification ratio r^+ is the ratio of the current density at the two opposite polarities, and the reported rectification ratio is an average of rectification ratios for

all junctions. The histogram was plotted based on the data set of measured values of r^+ at a given voltage, and then fitted with Gaussian curves to obtain standard deviation of $\log|r^+|$.

CV Measurements. We fabricated the samples in the same way as the samples used for J-V measurements, and measured the cyclic voltammograms using a three-electrode cell in an aqueous 0.1 M $KClO_4$, with a scan rate of 100 mV/s. A template-stripped Au surface (with a SAM on its surface) serves as the working electrode, and a Pt wire as the counter electrode. We prepared the reference electrode as reported previously (AgCl-coated Ag wire immersed in an aqueous solution of 1.0 M KCl, with the reference solution separated from solution in contact with the sample by a porous glass frit).[8]

XPS Measurements. We used XPS to characterize the SAMs of BIPY-Co and BIPY-Cu with instruments located in the Center for Nanoscale System at Harvard University. The energy of the incident X-ray beam used by the Thermo Scientific K-Alpha XPS system is at 1486.6 eV. We recorded the high-resolution XPS spectra of S 2p, C 1s, N 1s, Au 4f, and Cu 2p. In analysis, we used the least-square peak fit with a pseudo-Voigt function (a linear combination of Lorentzian (30 %) and Gaussian (70 %) functions)[9] to fit the XPS spectra with XPSpeak software,[10] and the sloping background was modeled using a Shirley plus linear background correction.[11] The pseudo-Voight functions is used because it is well-known that instrumental factors (e.g., resolution of the analyzer or monochromator) and experimental factors (e.g., surface roughness of the samples, vibrational effect, and polarization effects) manifest themselves as Gaussian broadening of the ideally Lorentzian signals of photoelectrons.[12]

We calculated elemental ratios from the ratios of integrated area of XPS spectrum, and expect the reason that the uncorrected atomic ratios of nitrogen to sulfur is higher than two (Table 1) is because the probability of photoelectron emission from the sulfur atom reaching the

detector is lower than that of nitrogen, due to the density and thickness of the SAMs. We corrected the atomic ratios of nitrogen to sulfur with thickness of SAMs based on the exponential attenuation of signal intensity by the thickness of SAMs.[13,14] All uncertainties for XPS are based on standard deviation of seven results.

UPS Measurements. We measured work functions (WF) and HOMO energy using the UPS function installed in the Thermo Scientific K-Alpha XPS system. The samples were held on a specially designed biasing stage that is in electrical contact with the analyzer. We applied -30 V to the stage to accelerate the secondary electrons with sufficient kinetic energy to escape from surface and to be seen as a secondary electron peak. The WFs of SAM-modified Au^{TS} surfaces were calculated by the energy difference between the cut-off of the secondary electron peak and the middle of the Fermi edge. The HOMO level was determined by the energy position of the first peak next to the Fermi edge.

DFT Calculations. All calculations were performed using the Gaussian suite of software (G09, RevA.02).[15] Visualization of the geometries and molecular orbitals was performed with GaussView v5.0. Optimizations frequency analyses were carried out in the gas phase with the hybrid uB3LYP functional employing the LANL2DZ basis set.

Preparation of Junctions for Experiments at Different Temperature. We follow the method reported in the literature for the fabrication of molecular junctions used in temperature-experiments.[16] EGaIn tip contacted gently with the samples (Au^{TS}-$S(CH_2)_{11}$BIPY-M) with the contact area of ~ 900 μm^2. As a drop of photocurable polymer (Norland Optical Adhesive 61, Norland Products) was placed on the samples near the EGaIn electrode to encapsulate and prevent the condensation of water, the Au^{TS}-$S(CH_2)_{11}$BIPY-M//Ga_2O_3/EGaIn junction was surrounded by the photocurable polymer. As we exposed the junctions to UV light using a hand-

held lamp for a few seconds (~5 s), the EGaIn electrode in conical shape was encapsulated with the cured polymer. Then, we gently lifted the syringe containing EGaIn to form encapsulated BIPY-M junctions.

Complexation of Metal with 2,2'-Bipyridine

2,2'-bipyridine (purchased from Sigma-Aldrich), which is one of the symmetrical isomers of bipyridine, has robust redox stability and can be easily functionalized.[17] 2,2'-bipyridine, thus, has been widely used in coordination chemistry as a metal chelating ligand.[18] Metal(II) forms three different metal complexes in stoichiometries of 1:1, 1:2, or 1:3 with 2,2'-bipyridine depending on concentrations in solution.[19,20] In BIPY-M junctions (Au^{TS}-$S(CH_2)_{11}$BIPY-M), metal(II) ions formed complexes with SAMs of alkanethiolates terminated by 2,2'-bipyridine with 1:1 stoichiometry. According to the Irving-Williams order, cobalt and copper has a relatively stable structure on 1:1 complexation with 2,2'-bipyridine.[21] BIPY-Co and BIPY-Cu complex have a distorted tetrahedral structure.[17,22,23] Figure S1 shows two possible arrangements of BIPY-M SAMs with a 1:1 BIPY·M^{2+} complex. We believe that the *cis*-conformation (Figure S1a) is more probable than the *trans*-conformation (Figure S1b) for two reasons: i) the ease with which metals are incorporated into the SAM suggest the BIPY ligand is readily available for binding at the surface of the SAM, ii) the generally accepted bonding geometry at sulfur (120° angular geometry for divalent sulfur), for an alkane thiol bound to a Au^{TS} surface, is compatible with the *cis*-conformation and not the *trans*-conformation.

Choice of Electrodes

Template-stripped Au surfaces (Au^{TS}) served as bottom electrodes. Molecules (i.e., $S(CH_2)_{11}BIPY$) align on the Au surface, and form SAMs.[24] The surface roughness and defects can distort the result of tunneling by creating an undesired tunneling path other than the tunneling along the molecules that we want to analyse. We, thus, used ultraflat Au^{TS} to minimize the defects of the surface; the root-mean-square roughness for Au^{TS} surface was 5.1 ± 0.4 nm (over an area of 25 μm^2).[1] GaO_x/EGaIn served as a top electrode which enables non-damaging soft contact, as well as the simple and rapid measurements of current.[2] Native oxide layer (a few atomic layers thick) of EGaIn results in the non-Newtonian behavior of GaO_x/EGaIn—because GaO_x/EGaIn maintains the conical shape and is not a (hard) solid—which (i) allows the measurements under ambient conditions, and (ii) does not penetrate the SAMs with high yield (70-90%).[2]

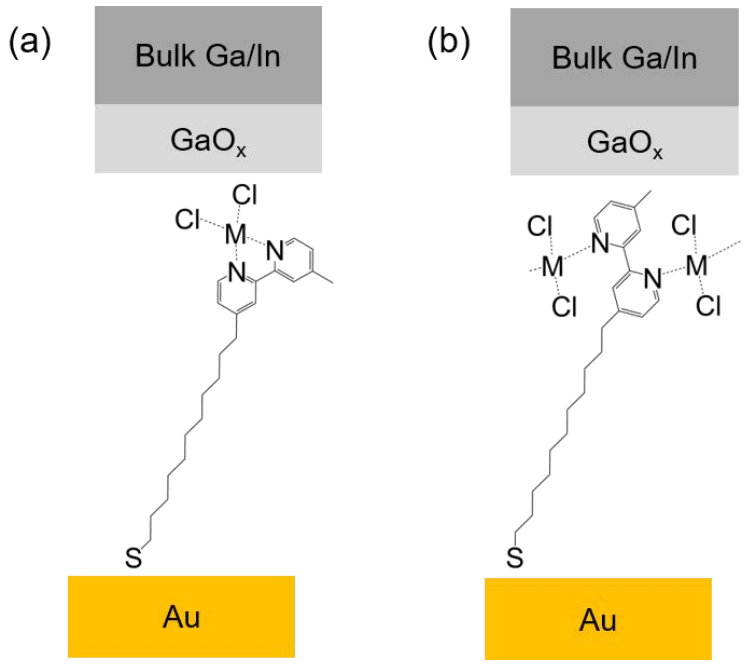

Figure S1.Schematic images of the molecular junction with the structures of Au^{TS}-$S(CH_2)_{11}$BIPY-MCl_2//GaO_x/EGaIn in which the BIPY groups are (a) *cis*-oriented, or (b) *trans*-oriented. We believe that the *cis*-conformation is more probable than the *trans*-conformation (see main text).

Statistical Analysis

Figure 2c shows the histograms of $\log|r^+|$ measured at ±1.0 V for the BIPY-Co and BIPY-Cu junctions. The standard deviations of $\log|r^+|$ are represented by σ_{log}. The histograms are fitted with Gaussian curves to obtain the mean values and the standard deviations. Yields—defined by the ratio of working junctions to the total number of junctions—in BIPY-Co and BIPY-Cu juctions are 84% and 80%, respectively. The standard deviation (σ_{log}) of $\log|r^+|$ in BIPY-Co junctions is =0.33 and that in BIPY-Cu junctions is 0.1. We assign this difference to the difference of conduction mechanisms at ±1.0 V in both junctions. In FN tunneling conditions (e.g., BIPY-Co junctions at -1.0 V) where electron tunnels from the Fermi level of electrodes to the LUMO of alkyl chain, the shape of tunneling barrier determines the width of tunneling barrier. In the case of direct tunneling conditions (e.g., BIPY-Cu junctions at -1.0 V) where electron tunnels between the Fermi level of Au surface and molecular orbitals of BIPY group, while, the width of tunneling barrier is not strongly affected by the shape of tunneling barrier. Thus, the (sample-to-sample or junction-to-junction) deviation in the shape of tunneling barrier—which can be caused by the defects in SAMs or Au^{TS} electrode[5]—could change the width of tunneling barrier in FN tunneling conditions more than that in direct tunneling conditions.

Oxidation State of BIPY-Cu moiety

One notable point is that the reduction potential of Au^{TS}-$S(CH_2)_{11}$BIPY-Cu shown in CV and UPS results is within the range defined by the Fermi level of EGaIn at ±1.0 V. That is, BIPY-Cu moiety reduces and oxidizes during the measurement of the tunneling current, approximately, at +0.80 ± 0.05 V. The oxidation state of BIPY-Cu complexes is +1 at -1.0 V, and +2 at +1.0 V if

we assume that all BIPY-Cu complexes fully reduce and oxidize. Details on the redox reaction of BIPY group, however, will not be discussed in this work because the redox reaction is not the origin of rectification characteristics in BIPY-based molecular junctions (see main text).

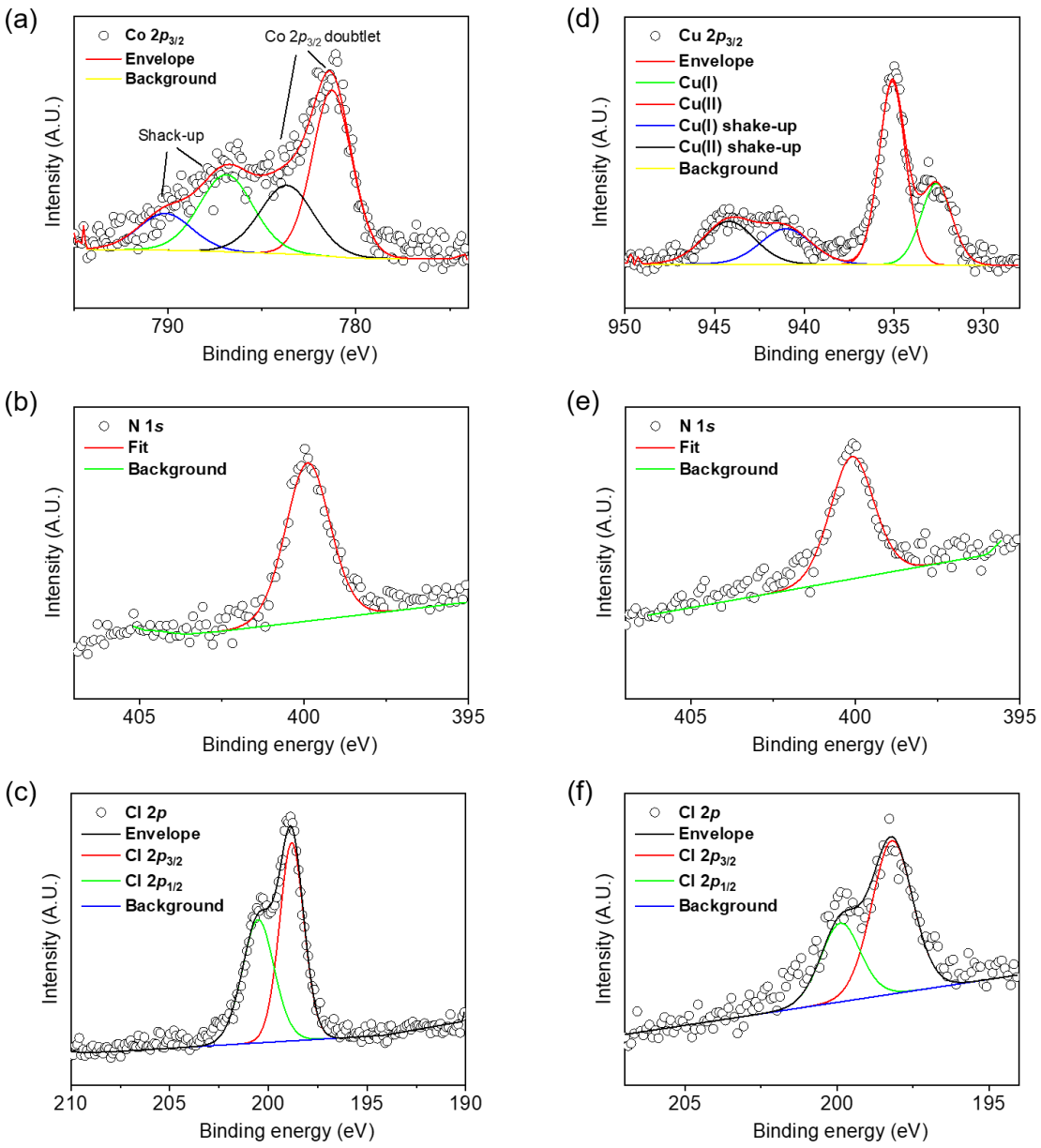

Figure S2. (a) Co $2p_{3/2}$ (b) N 1*s* and (c) Cl 2*p* X-ray photoelectron spectroscopy (XPS) spectra for $S(CH_2)_{11}$BIPY-Co SAMs on Au^{TS}. (d) Cu $2p_{3/2}$ (e) N 1*s* and (f) Cl 2*p* XPS spectra for $S(CH_2)_{11}$BIPY-Cu SAMs on Au^{TS}.

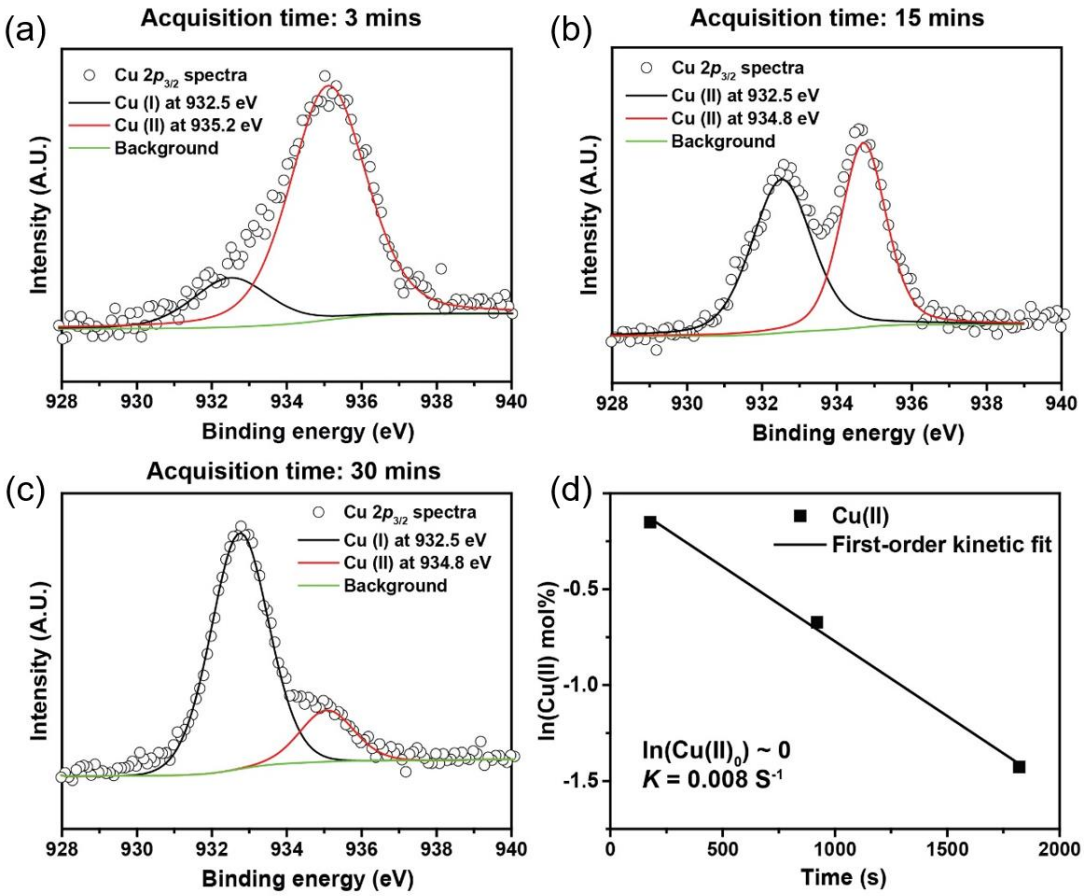

Figure S3. Cu $2p_{3/2}$ X-ray photoelectron spectroscopy (XPS) spectra for $S(CH_2)_{11}$BIPY-Cu SAMs on Au^{TS} as a function acquisition time: (a) 3 mins, (b) 15 mins, and (c) 30 mins. Figure 3d show decreased Cu(II) mol% as a function of acquisition time. The oxidation state of BIPY-Cu complex of as-fabricated BIPY-Cu junctions is +2.

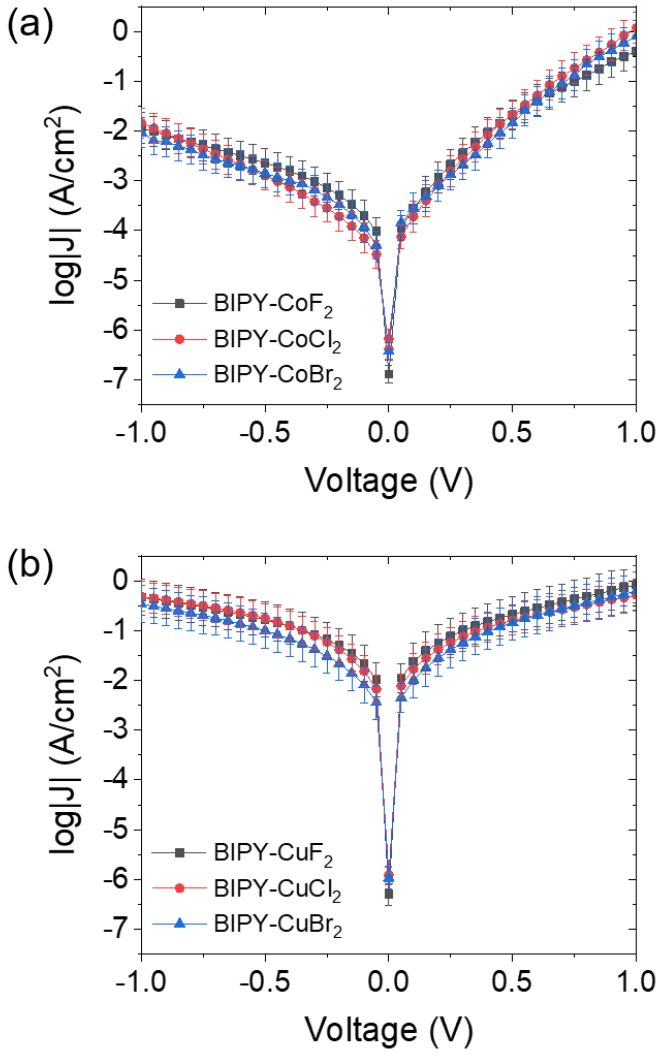

Figure S4. The semi-log plots of averaged J(V) traces of BIPY-Co and BIPY-Cu junctions which complexed with halide anions.

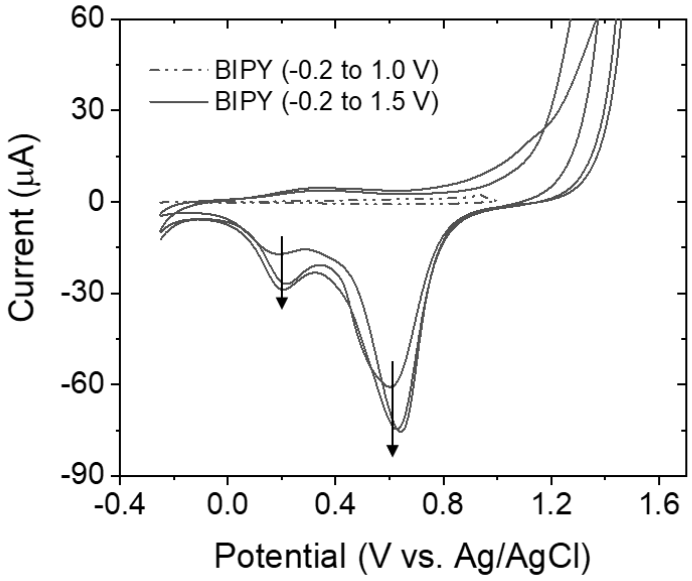

Figure S5. Cyclic voltammograms of SAMs of $S(CH_2)_{11}BIPY$ on template-stripped Au with different potential windows. The other measurement conditions are the same as the measurement conditions in Figure 3. With larger potential window (blue line), new peaks with increasing peak height appeared in the CV. We think that defects in the SAMs created by SAMs coming off the Au surface due to the high applied potential could cause these irreversible peaks.[25,26]

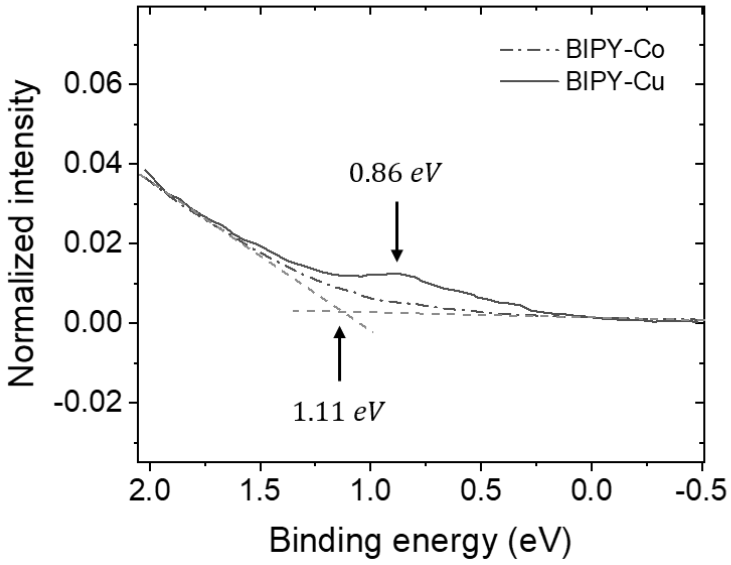

Figure S6. Ultraviolet photoelectron spectroscopy (UPS) analysis for $S(CH_2)_{11}$BIPY-Co and $S(CH_2)_{11}$BIPY-Cu SAMs on Au^{TS}. The values of binding energy of $S(CH_2)_{11}$BIPY-Co and $S(CH_2)_{11}$BIPY-Cu SAMs are 1.11 eV and 0.86 eV, respectively. The error bar of the HOMO is 0.05 eV; that is the photon energy resolution of the UPS spectra.

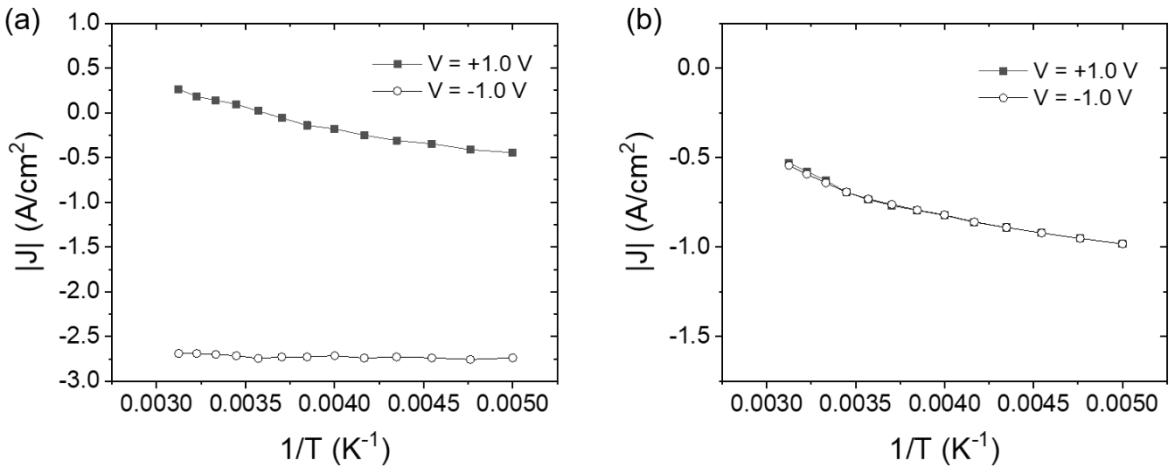

Figure S7. Arrhenius plots of (a) BIPY-Co junction and (b) BIPY-Cu junction for values of current density measured at +1.0 V and -1.0 V as a function of temperature.

Mechanism of Charge Transport

The "Simmons equation" proposed by Simmons describes the mechanism of charge transport across the tunneling barrier (eq. 1).

$$J = \frac{q}{4\pi^2\hbar d^2}\left[\left(\Phi_B - \frac{eV}{2}\right)\exp\left(-\frac{2d\sqrt{2m}}{\hbar}\sqrt{\Phi_B - \frac{eV}{2}}\right)\right.$$
$$\left. - \left(\Phi_B + \frac{eV}{2}\right)\exp\left(-\frac{2d\sqrt{2m}}{\hbar}\sqrt{\Phi_B + \frac{eV}{2}}\right)\right], \qquad (1)$$

where q is the electronic charge, d is the barrier width (Å), Φ_B is the average barrier height (eV), V is the applied voltage, and m is the effective mass of electron (kg).[27–31] In molecular junctions, the molecular orbitals (e.g., the LUMO of alkane chain) determine the shape of tunneling barrier. Thus, the barrier width corresponds to the thickness of SAMs (i.e., the length of $S(CH_2)_{11}$BIPY-M), and the barrier height is the energy offset between the Fermi level of electrode and the nearest molecular orbital.

At low-voltages ($eV \ll \Phi_B$), the barrier height is considered to be the zero-voltage mean barrier height—barrier shape is rectangular—and the charge tunnels directly through the whole tunneling barrier (Figure S8a). In these circumstances, tunneling is called direct tunneling. For direct tunneling,[27–31] Eq. (1) reduces to Eq. (2)

$$J_{DT} \sim V\exp\left(-\frac{2d}{\hbar}\sqrt{2m\Phi_B}\right). \qquad (2)$$

The current density is proportional to applied voltage. The junction, thus, shows Ohmic behavior for low voltages. Direct tunneling is indicated by a logarithmic growth of $\ln(J/V^2)$ with 1/V in Fowler-Nordheim (FN) plots. As the applied voltage increase ($eV \approx \Phi_B$), an applied voltage reaches transition voltage at which the Fermi level of electrode is aligned with the barrier height

of the opposite junction. In the high-voltage range ($eV > \Phi_B$), charge does not tunnel directly to the other side of the barrier (Figure S8b), but tunnels from the Fermi level of the electrode to the LUMO level of the alkane chain (i.e., a part of the tunneling barrier) because the energy level of the charges is higher than the barrier height of the opposite side (Fowler-Nordheim (FN) tunneling). In FN tunneling conditions,[27–31] Eq. (1) reduces to Eq. (3)

$$J_{FN} \sim V^2 \exp\left(-\frac{4d}{3q\hbar V}\sqrt{2m\Phi_B^3}\right). \quad (3)$$

The FN tunneling is indicated by a linear decay in FN plots.

Hopping conduction is defined as the inelastic transfer of an electron between two localized electronic states centered at different locations. The magnitude of current density via hopping conduction is proportional to applied voltage difference and generally depends on temperature.[32–34]

$$J_{HC} \sim V\, exp\left(-\frac{\Phi_B}{kT}\right). \quad (4)$$

Thus, FN plot allows us to distinguish whether the mechanism of tunneling is direct tunneling or FN tunneling, and we are able to know if hopping conduction is involved in the charge transport across the molecular junctions by investigating the temperature-dependence. Quantitative analysis based on the Simmons model may result in incorrect interpretation—e.g., the prediction of the exact value of barrier height—because this model neglects the effects of potential drop across the contact, and the effects of round off at the edge of potential barrier. This model, however, provides a reliable method for distinguishing the mechanism of tunneling if the junction shows a clear linear decay and the applied voltage is sufficiently larger than the transition voltage.[35]

In summary, FN plots indicate when the tunneling currents proceed by a direct tunneling mechanism, where charge tunnels through the whole tunneling barrier, (indicated by a logarithmic growth of $\ln(J/V^2)$ on 1/V), or by a FN tunneling mechanisms where charge tunnels through only part of the tunneling barrier (indicated by a linear decay).

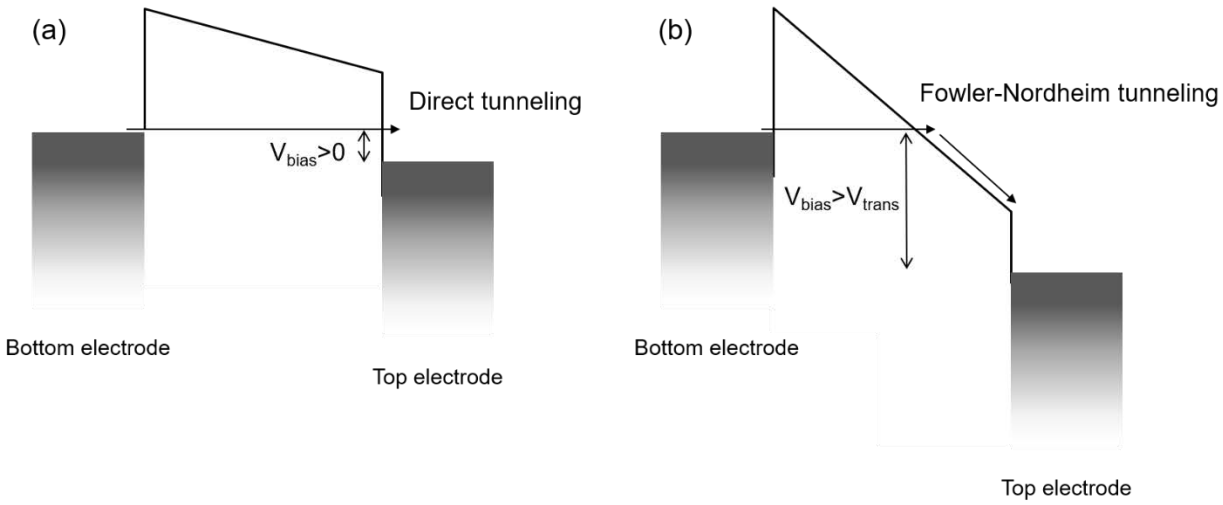

Figure S8. Schematic representation of energy level diagrams in conditions of (a) direct tunneling and (b) FN tunneling.

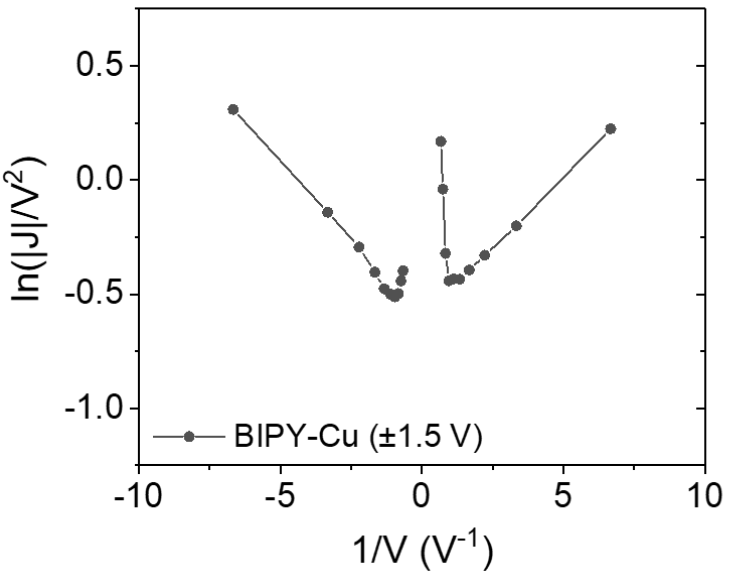

Figure S9. FN plot for the BIPY-Cu junctions with ±1.5 V applied voltage window. BIPY-Cu junctions start to show the transition of the conduction mechanism.

Rectification in BIPY-M junctions with First Row Transition Metals

To verify our hypothesis, we characterized the rectification in BIPY-M junctions with first-row transition metals (where M = Cr, Mn, Fe, Co, Ni, or Cu) to confirm if the hypothesis holds for the other transition metal. To minimize uncertainties, (i) all the BIPY-M junctions are complexed with metals which have the same principal quantum number, (ii) the oxidation state of metals in as-fabricated BIPY-M junctions is +2, and (iii) the counterions are all chloride ions.

Measurements of HOMO levels using UPS and DFT calculations. Using ultraviolet photoelectron spectroscopy (UPS), we measured HOMO levels of the $S(CH_2)_{11}$BIPY-M SAMs on a Au^{TS} surface (Figure S10). Our UPS measurements were performed relative to a Au surface as a standard, meaning the x-axis represents the Fermi level of Au. Therefore, a binding energy of zero corresponds to -4.3 eV, and a HOMO level of 1.0 eV (vs. Au) equals a HOMO level of -5.3 eV with respect to vacuum. Based on our UPS results, the HOMOs in BIPY-M junctions are as follows: BIPY-Cr (-0.96 eV), BIPY-Mn (-1.14 eV), BIPY-Fe (-1.10 eV), BIPY-Co (-1.11 eV), BIPY-Ni (-1.11 eV), and BIPY-Cu (-0.86 eV) (Figure S10). Values are reported relative to Au.

To cross-check the HOMO levels measured by UPS, we calculated the molecular orbitals using density functional theory (DFT) calculations (Figure S10). The results of the DFT calculations show the same trend in HOMO levels as the UPS measurements, and agree with our hypothesis that rectification is caused by the accessibility of the HOMO level in BIPY-Cr and BIPY-Cu junctions, at -1.0 V. Meanwhile, because the HOMO levels of the other BIPY-M junctions are inaccessible at -1.0 V, their rectification ratios will be higher than BIPY-Cr and BIPY-Cu junctions.

Electrical characterization of the junctions. Figures S10 shows averaged current density values (versus applied voltage) measured for BIPY-M junctions: BIPY-Cr (399 traces,

one trace from -1.0 V to 1.0 V), BIPY-Mn (378 traces), BIPY-Fe (399 traces), BIPY-Co (548 traces), BIPY-Ni (399 traces), and BIPY-Cu (336 traces). As predicted, BIPY-Cr (r^{+}=1.90), which have high-lying HOMO (>-5.3 eV) like BIPY-Cu junctions, do not rectify current—we consider rectification ratios < 5 to signify 'non-rectifying' junctions, because such small values might originate from artifacts associated with the experimental setup. According to our hypothesis, these junctions (BIPY-Cr and BIPY-Cu) have the same rectification properties because in each case, the tunneling width at opposite polarities are the same. The other BIPY-M junctions whose HOMO is lower than -5.3 eV, however, rectify current (Figure S11), because their HOMOs are inaccessible at -1.0 V, and thus the widths of the tunneling barriers are different at opposite polarities. The results show that the relative position of HOMO with respect to the Fermi level of Au determines the rectification in BIPY-M junctions, while the rectification in BIPY junction without metal depends on Fermi level pinning.[36]

Fowler-Nordheim (FN) plots analysis. According to our hypothesis, if the HOMO of a BIPY-M junction is higher than the Fermi level of the Au surface, the mechanism of tunneling at -1.0 V will be direct tunneling, because the electron tunnels from the BIPY-centred HOMO through the entire width of the alkyl chain. As predicted, FN plots support the inferences based on our hypothesis (Figure S12). The mechanism of tunneling at -1.0 V in BIPY-Cr and BIPY-Cu junctions, in which molecular orbitals are *equally* involved in tunneling at -1.0 V, show no transition of conduction mechanism. The conduction mechanisms of tunneling in the all other BIPY-M junctions (BIPY-Mn, BIPY-Fe, BIPY-Co, and BIPY-Ni) which have a relatively low-lying HOMOs, however, transitioned from direct tunneling to FN tunneling in the negative bias range.

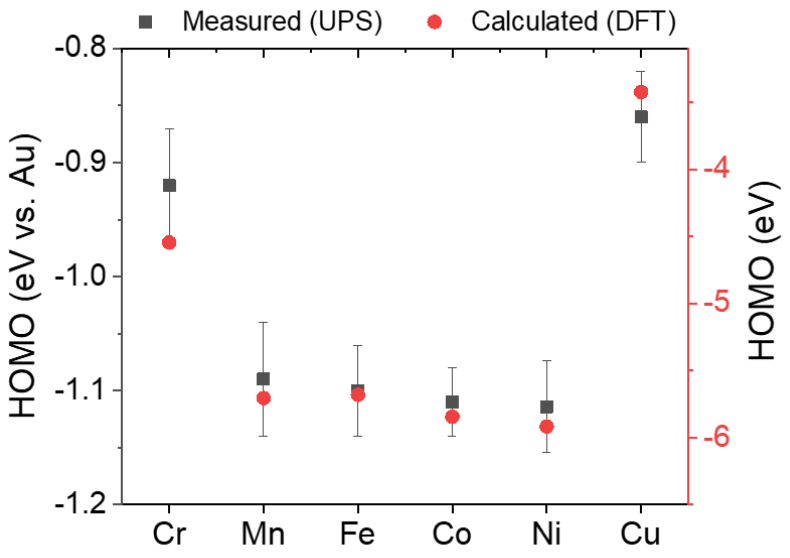

Figure S10. HOMO levels of BIPY-M complexes (i) measured by UPS (black squares) relative to a Au surface, and (ii) calculated using DFT (uB3LYP/LanL2DZ) (red circles). The oxidation state of metals in as-fabricated BIPY-M junctions is +2, and the counterions are all chloride ions.

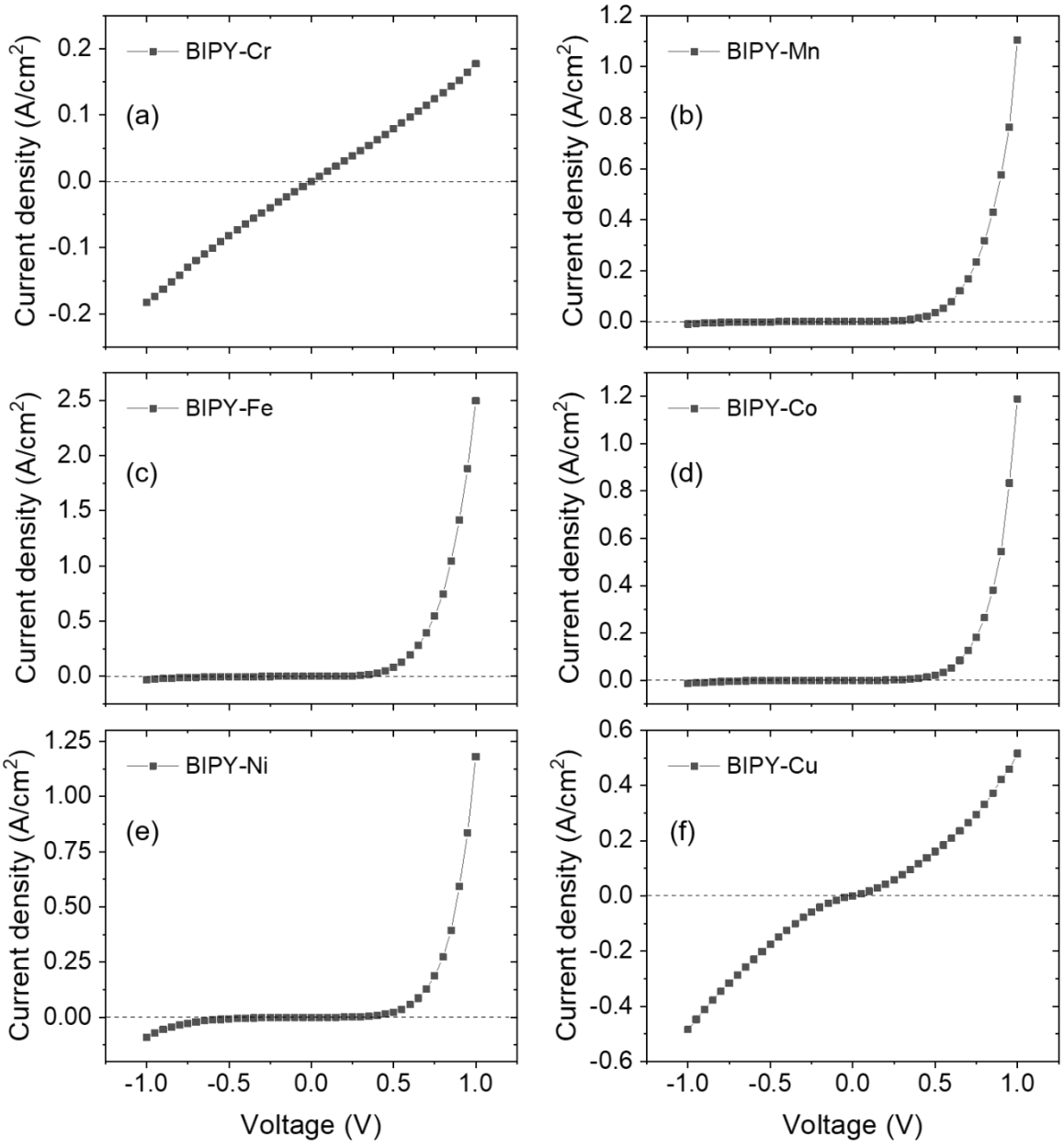

Figure S11. Averaged J(V) traces of (a-f) Au^{TS}-$S(CH_2)_{11}$BIPY-M//GaO_x/EGaIn junctions (M = (a) Cr, (b) Mn, (c) Fe, (d) Co, (e) Ni, and (f) Cu).

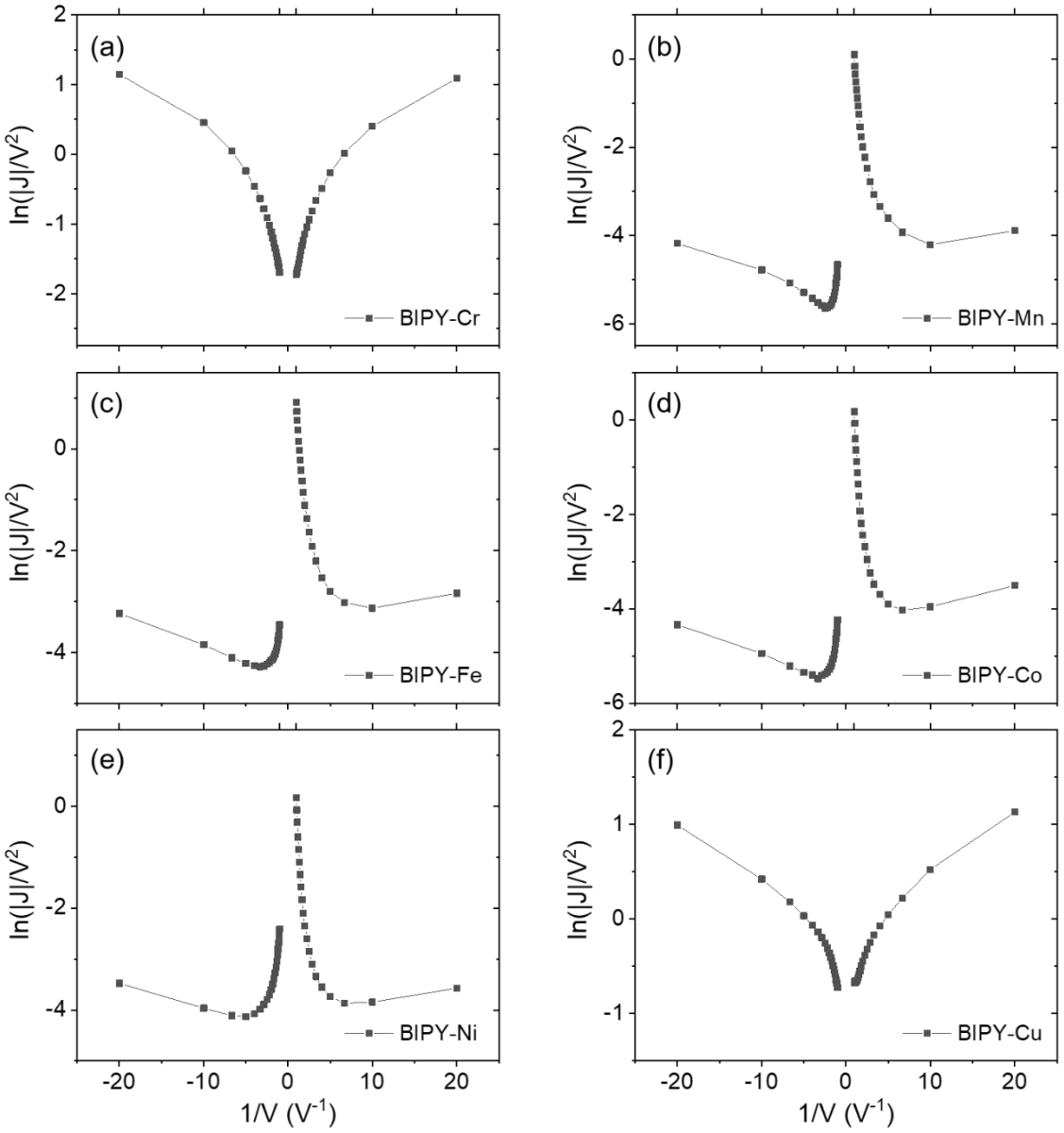

Figure S12. Fowler-Nordheim (FN) plots in BIPY-M junctions. There is one-to-one correspondence with Figure S11. No transition is observed in BIPY-Cr, and BIPY-Cu junctions.

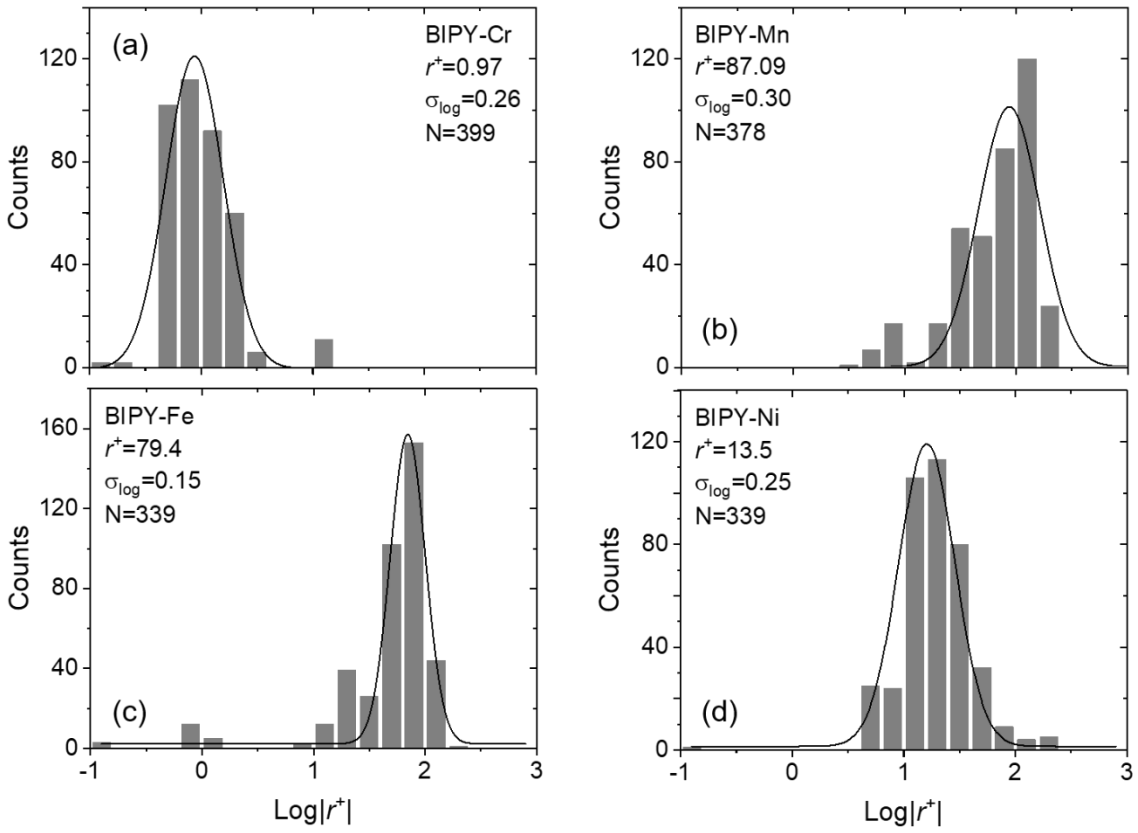

Figure S13. The histograms of log|r^+| of the BIPY-M junctions at ±1.0 V with a Gaussian fit to the histograms (M = (a) Cr, (b) Mn, (c) Fe, and (d) Ni).

Table S1. Elemental ratios in the Au^{TS}-$S(CH_2)_{11}$BIPY-M junctions characterized by XPS.

	BIPY-Cr	BIPY-Mn	BIPY-Fe	BIPY-Ni
Sulfur : Nitrogen	1 : 2.83 ± 0.03	1 : 2.91 ± 0.07	1 : 2.86 ± 0.08	1 : 2.72 ± 0.07
Metal : Nitrogen	1 : 2.22 ± 0.18	1 : 1.79 ± 0.16	1 : 1.88 ± 0.15	1 : 2.21 ± 0.12
Metal : Chloride	1 : 1.13 ± 0.10	1 : 1.32 ± 0.11	1 : 1.54 ± 0.09	1 : 1.17 ± 0.05

DFT calculated geometries and thermochemical data

a. BIPY-Co

---

opt=calcfc freq=noraman ub3lyp/lanl2dz geom=connectivity

Zero-point correction= 0.362376 (Hartree/Particle)

Thermal correction to Energy= 0.387220

Thermal correction to Enthalpy= 0.388164

Thermal correction to Gibbs Free Energy= 0.301220

Sum of electronic and zero-point Energies= -955.311635

Sum of electronic and thermal Energies= -955.286792

Sum of electronic and thermal Enthalpies= -955.285847

Sum of electronic and thermal Free Energies= -955.372791

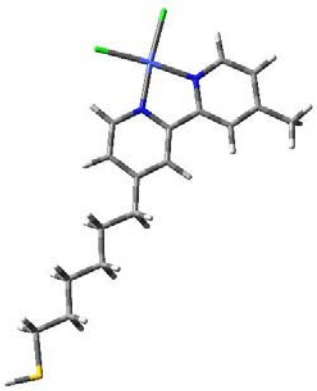

0 2

C	5.04223200	2.71410000	0.01588100	H	-2.53434100	1.55439600	0.77654200
C	3.86680800	3.49645800	-0.00861900	H	-2.54289800	1.47588400	-0.97615700
C	4.96125100	1.31611800	0.02657500	C	-3.61519000	-0.14625000	-0.02083400
C	2.63775300	2.80782500	-0.02461000	H	-3.53455500	-0.76798800	0.88369400
H	5.83545000	0.67422000	0.04694900	H	-3.55844600	-0.82911600	-0.88196000
C	2.61077400	1.40311700	-0.01279100	C	-4.98633300	0.56277300	-0.02846200
H	1.70906600	3.36808100	-0.04801500	H	-5.04876100	1.24685100	0.83282600
C	1.37754400	0.59123300	-0.02773600	H	-5.06866800	1.18912500	-0.93105000
C	0.07887200	1.11731900	-0.04219300	C	-6.17500100	-0.42166700	0.01688900
C	0.53162200	-1.60147300	-0.03199100	H	-6.09528400	-1.04792400	0.91946000
C	-1.04459600	0.26096900	-0.05157100	H	-6.11593600	-1.10428200	-0.84548900
H	-0.06937700	2.19282800	-0.04453500	C	-7.54177600	0.30071000	0.00982800
C	-0.78840000	-1.12504600	-0.04524400	H	-7.60215600	0.97885400	0.87347700
H	0.77452500	-2.65879600	-0.03011800	H	-7.62206500	0.92386400	-0.89276400
H	-1.59711000	-1.84601700	-0.05023400	C	-8.71863400	-0.68628500	0.05339900
N	3.76713000	0.66579600	0.01250900	H	-8.69078900	-1.29141200	0.96514400
N	1.59965500	-0.76491900	-0.02320900	H	-8.71068800	-1.34584600	-0.82016100
C	3.92977500	5.00776300	-0.00263600	S	-10.35419900	0.30006900	0.04170800
H	4.22914900	5.37822800	0.98744800	H	-11.20750400	-0.78314700	0.08561600
H	4.67000700	5.37546200	-0.72343300	Cl	5.73351900	-1.72079800	0.12302600
H	2.96119700	5.45584200	-0.24824300	Cl	3.01872300	-3.51266000	-0.07901600
H	6.02134600	3.18366200	0.02588900	Co	3.51034300	-1.30314100	0.00824300
C	-2.44500800	0.85626800	-0.07056100				

b. BIPY–Cu

---

opt=calcfc freq=noraman ub3lyp/lanl2dz geom=connectivity

Zero-point correction= 0.361701 (Hartree/Particle)

Thermal correction to Energy= 0.387804

Thermal correction to Enthalpy= 0.388749

Thermal correction to Gibbs Free Energy= 0.298682

Sum of electronic and zero-point Energies= -1006.363943

Sum of electronic and thermal Energies= -1006.337839

Sum of electronic and thermal Enthalpies= -1006.336895

Sum of electronic and thermal Free Energies= -1006.426962

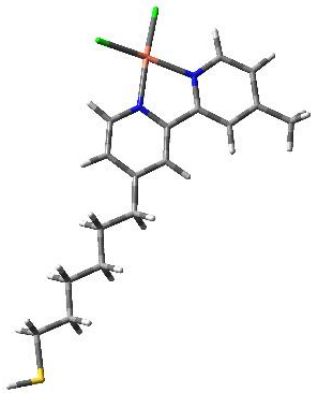

0 2

C	4.98756200	2.78262500	-0.07695500	H	-2.57945100	1.55004300	0.82679900
C	3.79890900	3.54484800	-0.10760800	H	-2.59354400	1.48313400	-0.92630100
C	4.91973500	1.38285900	-0.03019800	C	-3.65872200	-0.14798800	0.02179100
C	2.57535000	2.84319500	-0.08767600	H	-3.57952100	-0.76878700	0.92710900
H	5.79962900	0.74970000	0.02087200	H	-3.59726100	-0.83128100	-0.83868200
C	2.56670400	1.43743100	-0.04910500	C	-5.03193700	0.55696500	0.00969100
H	1.64209100	3.39618500	-0.10169900	H	-5.09846900	1.24274900	0.86931400
C	1.33255100	0.60998800	-0.02920000	H	-5.11412200	1.18100700	-0.89448300
C	0.03047000	1.13136000	-0.03825900	C	-6.21758700	-0.43114700	0.05441700
C	0.49324600	-1.58622400	0.01128900	H	-6.13894600	-1.05400200	0.95944400
C	-1.08855500	0.26686200	-0.01504700	H	-6.15331900	-1.11655100	-0.80537500
H	-0.12752400	2.20520800	-0.06302600	C	-7.58670200	0.28663400	0.04006900
C	-0.83183900	-1.11908100	0.01217400	H	-7.65239500	0.96765500	0.90106100
H	0.74405500	-2.64215100	0.00538300	H	-7.66594900	0.90625800	-0.86503300
H	-1.63975300	-1.84062900	0.02830400	C	-8.76038400	-0.70417100	0.08304100
N	3.73321900	0.72940100	-0.02275800	H	-8.73378900	-1.30589100	0.99707900
N	1.54727200	-0.74017000	-0.00382600	H	-8.74706800	-1.36688500	-0.78807000
C	3.84043800	5.05583400	-0.17496200	S	-10.39917400	0.27659200	0.06184500
H	4.59490300	5.46252100	0.50874500	H	-11.24894700	-0.80940100	0.10538200
H	4.10593000	5.38923500	-1.18773200	Cu	3.53430900	-1.33622100	0.01683400
H	2.87242000	5.50038900	0.07927700	Cl	5.68453900	-1.68456900	0.72390100
H	5.95890500	3.26792100	-0.08271300	Cl	3.05740900	-3.47853600	-0.63897300
C	-2.49133800	0.85779000	-0.02530500				

c. BIPY–Cr

---

opt=calcfc freq=noraman ub3lyp/lanl2dz geom=connectivity

Zero-point correction= 0.361477 (Hartree/Particle)

Thermal correction to Energy= 0.387420

Thermal correction to Enthalpy= 0.388364

Thermal correction to Gibbs Free Energy= 0.298523

Sum of electronic and zero-point Energies= -896.496956

Sum of electronic and thermal Energies= -896.471013

Sum of electronic and thermal Enthalpies= -896.470069

Sum of electronic and thermal Free Energies= -896.559910

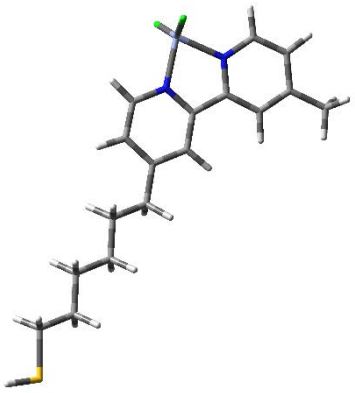

0 1

C	-5.26486000	2.33702100	0.24206800	H	2.42015700	1.09848800	-1.47070900
C	-4.14424600	3.20631500	0.13902000	H	2.37647000	1.65243900	0.19446200
C	-5.08541000	0.95656000	0.22093100	C	3.49408600	-0.18343000	-0.10099600
C	-2.87994900	2.61167800	0.02456800	H	3.51166500	-1.03009900	-0.80356800
H	-5.92527300	0.27444800	0.29852800	H	3.36216300	-0.60901000	0.90577800
C	-2.74751700	1.20780100	0.00835900	C	4.85007000	0.55009900	-0.17786200
H	-1.99410200	3.23472400	-0.05231700	H	4.95719100	1.01398200	-1.17166600
C	-1.50219600	0.46067100	-0.09044600	H	4.86290900	1.37335500	0.55370200
C	-0.20447800	0.99633900	-0.18956400	C	6.05492600	-0.38116100	0.07764100
C	-0.63152800	-1.72505500	-0.13895400	H	6.04344800	-1.19942500	-0.65961300
C	0.91777200	0.15282400	-0.27100700	H	5.94973500	-0.84998500	1.06895600
H	-0.07088300	2.07455000	-0.20403900	C	7.40743700	0.36339000	-0.00065400
C	0.67392100	-1.24509200	-0.23807400	H	7.51167300	0.82983600	-0.99114100
H	-0.85433700	-2.78444800	-0.12506900	H	7.42168900	1.17667200	0.73935000
H	1.48833600	-1.95782900	-0.28769800	C	8.59981800	-0.57337300	0.24751600
N	-3.85094300	0.38139900	0.10042300	H	8.63779500	-1.36788200	-0.50450100
N	-1.71560200	-0.90133600	-0.06851500	H	8.54873800	-1.02043800	1.24544700
C	-4.32541000	4.70853700	0.15138500	S	10.21689900	0.43685800	0.12955700
H	-4.93758300	5.03717300	-0.69935000	H	11.08720100	-0.60353200	0.38238000
H	-4.83805700	5.03662700	1.06536100	Cl	-3.85571600	-2.22203000	2.20742400
H	-3.36479100	5.23150800	0.09658300	Cl	-4.02376300	-1.91400300	-2.18850800
H	-6.26890100	2.74004900	0.33745100	Cr	-3.56722200	-1.56436300	0.02605600
C	2.31000700	0.74952500	-0.43084900				

d**. BIPY–Mn**

---

opt=calcfc freq=noraman ub3lyp/lanl2dz geom=connectivity

Zero-point correction= 0.362385 (Hartree/Particle)

Thermal correction to Energy= 0.387124

Thermal correction to Enthalpy= 0.388069

Thermal correction to Gibbs Free Energy= 0.301489

Sum of electronic and zero-point Energies= -914.132611

Sum of electronic and thermal Energies= -914.107872

Sum of electronic and thermal Enthalpies= -914.106927

Sum of electronic and thermal Free Energies= -914.193507

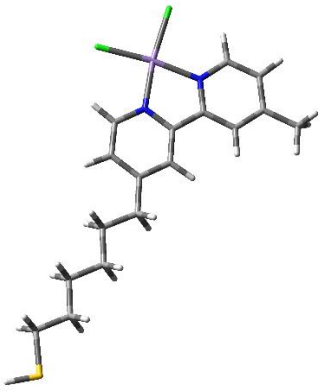

0 2

C	-5.04721200	2.73580800	-0.01670300	H	2.51240100	1.54014100	-0.80746300
C	-3.86103000	3.50803900	-0.00459400	H	2.51757600	1.48235400	0.94618500
C	-4.98249600	1.34112800	-0.01774600	C	3.58992400	-0.15133600	0.01213200
C	-2.64438300	2.80548700	0.00599000	H	3.51304900	-0.78120300	-0.88711700
H	-5.86960400	0.71894500	-0.02716900	H	3.52875700	-0.82651300	0.87906600
C	-2.62902200	1.39715800	0.00434800	C	4.96144000	0.55690700	0.01951700
H	-1.70900800	3.35471200	0.01572200	H	5.02795200	1.23320300	-0.84761500
C	-1.40634700	0.58316800	0.01451400	H	5.03975100	1.19153900	0.91668100
C	-0.10361400	1.10776900	0.02465600	C	6.15015400	-0.42798900	-0.01138100
C	-0.55321800	-1.60868700	0.01976600	H	6.07485000	-1.06212500	-0.90883400
C	1.01927000	0.25699600	0.03294100	H	6.08667200	-1.10309800	0.85660900
H	0.04267200	2.18349600	0.02565700	C	7.51704600	0.29420800	-0.00371400
C	0.76246400	-1.13194900	0.02958100	H	7.58187100	0.96477700	-0.87293900
H	-0.78381000	-2.66763800	0.01788300	H	7.59277300	0.92526500	0.89376500
H	1.57151100	-1.85268000	0.03429300	C	8.69392400	-0.69325800	-0.03273000
N	-3.79427900	0.66525800	-0.00740900	H	8.67063800	-1.30618600	-0.93938300
N	-1.63373400	-0.77669200	0.01252000	H	8.68140900	-1.34532700	0.84639900
C	-3.91196100	5.01971000	-0.00340000	S	10.32983400	0.29267500	-0.02106500
H	-4.43543500	5.39437300	-0.89284000	H	11.18298800	-0.79118000	-0.05056100
H	-4.45771100	5.39237200	0.87336900	Cl	-3.03531400	-3.58291000	0.01826500
H	-2.90950700	5.46008900	0.00972300	Cl	-5.84676600	-1.70799100	-0.04008000
H	-6.02138400	3.21591500	-0.02536400	Mn	-3.58298200	-1.35806600	-0.00438800
C	2.42010500	0.85233600	0.04778400				

e. BIPY–Fe

---

opt=calcfc freq=noraman ub3lyp/lanl2dz geom=connectivity

Zero-point correction= 0.362325 (Hartree/Particle)

Thermal correction to Energy= 0.388168

Thermal correction to Enthalpy= 0.389112

Thermal correction to Gibbs Free Energy= 0.299752

Sum of electronic and zero-point Energies= -933.644765

Sum of electronic and thermal Energies= -933.618922

Sum of electronic and thermal Enthalpies= -933.617978

Sum of electronic and thermal Free Energies= -933.707338

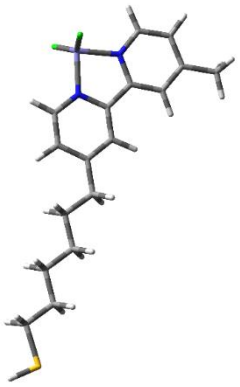

0 1

C	-5.31182200	2.28383100	-0.00067900	H	2.38584000	1.47203700	-0.87679400
C	-4.19811300	3.15794800	-0.00038500	H	2.38587200	1.47150700	0.87826600
C	-5.11699000	0.89959500	-0.00058600	C	3.50849000	-0.15936100	0.00022400
C	-2.91714800	2.57376400	-0.00010800	H	3.45860200	-0.81341400	-0.88365900
H	-5.94972700	0.20521100	-0.00081000	H	3.45876500	-0.81379600	0.88383400
C	-2.77534500	1.17599800	-0.00003600	C	4.85942300	0.58763500	0.00026700
H	-2.03482200	3.20574500	0.00003900	H	4.91316000	1.24509900	-0.88203400
C	-1.50296800	0.43553300	0.00014600	H	4.91329700	1.24475600	0.88281500
C	-0.22012600	0.99868600	0.00029200	C	6.07497400	-0.36448400	-0.00001300
C	-0.58873800	-1.73552800	0.00014900	H	6.02349000	-1.02072300	-0.88316800
C	0.92641500	0.17480200	0.00037000	H	6.02366300	-1.02102400	0.88292900
H	-0.10622300	2.07895700	0.00032900	C	7.42176800	0.39468100	-0.00001900
C	0.71479400	-1.22178500	0.00029400	H	7.47417000	1.04742900	-0.88351200
H	-0.77859400	-2.80315900	0.00008300	H	7.47434000	1.04714800	0.88367100
H	1.54664200	-1.91555900	0.00033700	C	8.62468600	-0.56136300	-0.00028200
N	-3.87469200	0.35603400	-0.00023600	H	8.62340700	-1.19406700	-0.89354000
N	-1.67416700	-0.92807800	0.00008000	H	8.62359800	-1.19431100	0.89280300
C	-4.38839100	4.65910200	-0.00009300	S	10.23400200	0.46753300	-0.00031500
H	-4.95667000	4.98286600	-0.88189600	H	11.11559300	-0.59377900	-0.00056300
H	-4.95059400	4.98313300	0.88553900	Cl	-3.78653700	-2.01799700	-2.19006100
H	-3.42992700	5.18851300	-0.00339900	Cl	-3.78651600	-2.01706600	2.19035100
H	-6.32425700	2.67621600	-0.00098400	Fe	-3.48366200	-1.50062600	0.00001700
C	2.31000200	0.81050100	0.00053600				

f. BIPY–Ni

---

opt=calcfc freq=noraman ub3lyp/lanl2dz geom=connectivity

Zero-point correction= 0.363024 (Hartree/Particle)

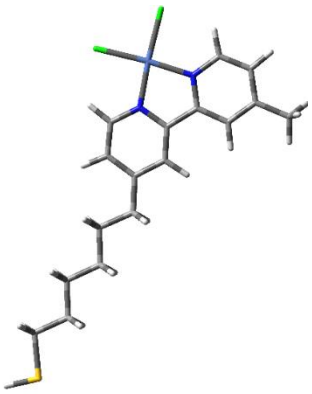

Thermal correction to Energy= 0.388444

Thermal correction to Enthalpy= 0.389388

Thermal correction to Gibbs Free Energy= 0.301814

Sum of electronic and zero-point Energies= -979.535621

Sum of electronic and thermal Energies= -979.510201

Sum of electronic and thermal Enthalpies= -979.509257

Sum of electronic and thermal Free Energies= -979.596831

0 2

C	-5.03954600	2.69554000	0.01292400
C	-3.86976700	3.48600600	0.00240900
C	-4.94975900	1.29780700	0.01499500
C	-2.63644900	2.80505900	-0.00920200
H	-5.82086000	0.65242800	0.02220700
C	-2.60156600	1.40091800	-0.00597000
H	-1.71046800	3.37015200	-0.02171100
C	-1.36748100	0.59433400	-0.01593500
C	-0.06964800	1.12143300	-0.02665100
C	-0.52264100	-1.59680700	-0.01865200
C	1.05415400	0.26564600	-0.03388000
H	0.07697900	2.19717300	-0.02868300
C	0.79750100	-1.11995400	-0.02919700
H	-0.76287500	-2.65410000	-0.01509600
H	1.60582000	-1.84133100	-0.03313300
N	-3.75221600	0.65641100	0.00609600
N	-1.58950300	-0.76073700	-0.01214400
C	-3.94250300	4.99673600	0.01923800
H	-4.68790400	5.36484600	-0.69590300
H	-4.24008300	5.35800600	1.01327700
H	-2.97772600	5.45271500	-0.22681100
H	-6.02204000	3.15796900	0.01851600
C	2.45447300	0.86102600	-0.04818000
H	2.55008200	1.49332900	-0.94514900
H	2.54575000	1.54721000	0.80848500
C	3.62469300	-0.14204500	-0.01508800
H	3.56345400	-0.81550300	-0.88331600
H	3.54860100	-0.77356400	0.88302700
C	4.99583900	0.56697900	-0.02152700
H	5.07409400	1.20272400	-0.91788600
H	5.06210200	1.24208300	0.84654000
C	6.18470800	-0.41776800	0.00831000
H	6.12176600	-1.09153200	-0.86074400
H	6.10916200	-1.05327500	0.90475700
C	7.55141800	0.30474700	0.00241400
H	7.62760800	0.93703000	-0.89416200
H	7.61563100	0.97411900	0.87260800
C	8.72848300	-0.68253000	0.03082300
H	8.71672100	-1.33336000	-0.84923100
H	8.70470600	-1.29674800	0.93658800
S	10.36399700	0.30395400	0.02169700
H	11.21747200	-0.77964100	0.05049400
Cl	-5.66043200	-1.72577800	0.02504700
Cl	-3.00861500	-3.46145100	-0.00175200
Ni	-3.47598400	-1.28155600	0.00405400

References to S.I.

(1) Weiss, E. A.; Kaufman, G. K.; Kriebel, J. K.; Li, Z.; Schalek, R.; Whitesides, G. M. Si/SiO2-Templated Formation of Ultraflat Metal Surfaces on Glass, Polymer, and Solder Supports: Their Use as Substrates for Self-Assembled Monolayers. *Langmuir* **2007**, *23* (19), 9686–9694.

(2) Chiechi, R. C.; Weiss, E. A.; Dickey, M. D.; Whitesides, G. M. Eutectic Gallium-Indium (EGaIn): A Moldable Liquid Metal for Electrical Characterization of Self-Assembled Monolayers. *Angew. Chemie - Int. Ed.* **2008**, *47* (1), 142–144.

(3) Yoon, H. J.; Liao, K. C.; Lockett, M. R.; Kwok, S. W.; Baghbanzadeh, M.; Whitesides, G. M. Rectification in Tunneling Junctions: 2,2'-Bipyridyl-Terminated n -Alkanethiolates. *J. Am. Chem. Soc.* **2014**, *136* (49), 17155–17162.

(4) Nijhuis, C. A.; Reus, W. F.; Whitesides, G. M. Molecular Rectification in Metal-SAM-Metal Oxide-Metal Junctions. *J. Am. Chem. Soc.* **2009**, *131* (49), 17814–17827.

(5) Nijhuis, C. A.; Reus, W. F.; Whitesides, G. M. Mechanism of Rectification in Tunneling Junctions Based on Molecules with Asymmetric Potential Drops. *J. Am. Chem. Soc.* **2010**, *132* (51), 18386–18401.

(6) Simeone, F. C.; Yoon, H. J.; Thuo, M. M.; Barber, J. R.; Smith, B.; Whitesides, G. M. Defining the Value of Injection Current and Effective Electrical Contact Area for Egain-Based Molecular Tunneling Junctions. *J. Am. Chem. Soc.* **2013**, *135* (48), 18131–18144.

(7) Reus, W. F.; Nijhuis, C. A.; Barber, J. R.; Thuo, M. M.; Tricard, S.; Whitesides, G. M. Statistical Tools for Analyzing Measurements of Charge Transport. *J. Phys. Chem. C* **2012**, *116* (11), 6714–6733.

(8) Semenov, S. N.; Belding, L.; Cafferty, B. J.; Mousavi, M. P. S.; Finogenova, A. M.; Cruz, R. S.; Skorb, E. V.; Whitesides, G. M. Autocatalytic Cycles in a Copper-Catalyzed Azide-Alkyne Cycloaddition Reaction. *J. Am. Chem. Soc.* **2018**, *140* (32), 10221–10232.

(9) Doniach, S.; Sunjic, M. Many-Electron Singularity in X-Ray Photoemission and X-Ray Line Spectra from Metals. *J. Phys. C Solid State Phys.* **1970**, *3* (2), 285.

(10) Wertheim, G. K.; Butler, M. A.; West, K. W.; Buchanan, D. N. E. Determination of the Gaussian and Lorentzian Content of Experimental Line Shapes. *Rev. Sci. Instrum.* **1974**, *45* (11), 1369–1371.

(11) Shirley, D. A. High-Resolution X-Ray Photoemission Spectrum of the Valence Bands of Gold. *Phys. Rev. B* **1972**, *5* (12), 4709.

(12) Olivero, J. J.; Longbothum, R. L. Empirical Fits to the Voigt Line Width. *J. Quant. Spectrosc. Radiat. Transf.* **1977**, *17*, 233–236.

(13) Jablonski, A.; Powell, C. J. Formalism and Parameters for Quantitative Surface Analysis by Auger Electron Spectroscopy and X-ray Photoelectron Spectroscopy. *Surf. Interface Anal.* **1993**, *20* (9), 771–786.

(14) Powell, C. J.; Jablonski, A. Electron Effective Attenuation Lengths for Applications in Auger Electron Spectroscopy and X-Ray Photoelectron Spectroscopy. *Surf. Interface Anal.* **2002**, *33* (3), 211–229.

(15) M. J. Frisch, G. W. Trucks, H. B. Schlegel, G. E. Scuseria, M. A. Robb, J. R. Cheeseman, G. Scalmani, V. Barone, B. Mennucci, G. A. Petersson, H. Nakatsuji, M. Caricato, X. Li, H. P. Hratchian, A. F. Izmaylov, J. Bloino, G. Zheng, J. L. Sonnenberg, M. Had, and D. J. F. Gaussian 09. Gaussian, Inc.: Wallingford CT 2009.

(16) Byeon, S. E.; Kim, M.; Yoon, H. J. Maskless Arbitrary Writing of Molecular Tunnel Junctions. *ACS Appl. Mater. Interfaces* **2017**, 40556–40563.

(17) Kaes, C.; Katz, A.; Hosseini, M. W. Bipyridine: The Most Widely Used Ligand. A Review of Molecules Comprising at Least Two 2,2′-Bipyridine Units. *Chem. Rev.* **2000**, *100* (10), 3553–3590.

(18) Balzani, V.; Juris, A.; Venturi, M.; Campagna, S.; Serroni, S. Luminescent and Redox-Active Polynuclear Transition Metal Complexes. *Chem. Rev.* **1996**, *96* (2), 759–833.

(19) Atkinson, G.; Baumann, J. E.; Arbor, A. The Thermodynamics of Chelation of 2 , 2 ’ - Bipyridine ; Technical Report Public Domain , Google-Digitized. **1961**.

(20) Irving, H.; Mellor, D. H. Mellor: The Stability of Metal Complexes of 1002. The Stability. *J Chem Soc* **1962**, No. 0, 5222–5237.

(21) Irving J. P., H. and W.; Irving, H. and Williams, J. P. Order of Stability of Metal Complexes. *Nature* **1948**, *162*, 746–747.

(22) Murali, M.; Palaniandavar, M. Mixed-Ligand Copper(II) Complexes with Positive Redox Potentials. *Transit. Met. Chem.* **1996**, *21* (2), 142–148.

(23) Angel, N. R.; Khatib, R. M.; Jenkins, J.; Smith, M.; Rubalcava, J. M.; Le, B. K.; Lussier, D.; Chen, Z. (Georgia); Tham, F. S.; Wilson, E. H.; et al. Copper (II) Complexes Possessing Alkyl-Substituted Polypyridyl Ligands: Structural Characterization and in Vitro Antitumor Activity. *J. Inorg. Biochem.* **2017**, *166* (Ii), 12–25.

(24) Weiss, E. A.; Chiechi, R. C.; Kaufman, G. K.; Kriebel, J. K.; Li, Z.; Duati, M.; Rampi, M. A.; Whitesides, G. M. Influence of Defects on the Electrical Characteristics of Mercury-Drop Junctions: Self-Assembled Monolayers of n-Alkanethiolates on Rough and Smooth Silver. *J. Am. Chem. Soc.* **2007**, *129* (14), 4336–4349.

(25) Diao, P.; Jiang, D.; Cui, X.; Gu, D.; Tong, R.; Zhong, B. Studies of Structural Disorder of Self-Assembled Thiol Monolayers on Gold by Cyclic Voltammetry and Ac Impedance. *J. Electroanal. Chem.* **1999**, *464* (1), 61–67.

(26) Che, G.; Li, Z.; Zhang, H.; Cabrera, C. R. Voltammetry of Defect Sites at a Self-Assembled Monolayer on a Gold Surface. *J. Electroanal. Chem.* **1998**, *453* (1–2), 9–17.

(27) Simmons, J. G. Electric Tunnel Effect between Dissimilar Electrodes Separated by a Thin Insulating Film. *J. Appl. Phys.* **1963**, *34* (9), 2581–2590.

(28) Simmons, J. G. Generalized Formula for the Electric Tunnel Effect between Similar Electrodes Separated by a Thin Insulating Film. *J. Appl. Phys.* **1963**, *34* (6), 1793–1803.

(29) Simmons, J. G. Conduction in Thin Dielectric Films. *J. Phys. D. Appl. Phys.* **1971**, *4* (5), 613–657.

(30) Beebe, J. M.; Kim, B.; Gadzuk, J. W.; Frisbie, C. D.; Kushmerick, J. G. Transition from Direct Tunneling to Field Emission in Metal-Molecule-Metal Junctions. *Phys. Rev. Lett.*

2006, *97* (2), 1–4.
(31) Seong, H. C.; Kim, B. S.; Frisbie, C. D. Electrical Resistance of Long Conjugated Molecular Wires. *Science (80-.).* **2008**, *320* (5882), 1482–1486.
(32) Nitzan, A. Electron Transmission through Molecules and Molecular Interfaces. *Annu. Rev. Phys. Chem.* **2001**, *52*, 681–750.
(33) Wang, W.; Lee, T.; Reed, M. A. Mechanism of Electron Conduction in Self-Assembled Alkanethiol Monolayer Devices. *Phys. Rev. B* **2003**, *68*, 035416.
(34) Lim, E. W.; Ismail, R. Conduction Mechanism of Valence Change Resistive Switching Memory: A Survey. *Electron.* **2015**, *4* (3), 586–613.
(35) Vilan, A.; Aswal, D.; Cahen, D. Large-Area, Ensemble Molecular Electronics: Motivation and Challenges. *Chem. Rev.* **2017**, *117* (5), 4248–4286.
(36) Kang, H.; Kong, G. D.; Byeon, S. E.; Yang, S.; Kim, J. W.; Yoon, H. J. Interplay of Fermi Level Pinning, Marcus Inverted Transport, and Orbital Gating in Molecular Tunneling Junctions. *J. Phys. Chem. Lett.* **2020**, 8597–8603.